Pergamon

PII : S0017–9310(97)00127–0

A bifurcation study of natural convection in porous media with internal heat sources : the non-Darcy effects

EUNGSOO CHOI† and A. CHAKMA

Department of Chemical and Petroleum Engineering, University of Calgary, Calgary, Alberta,
Canada T2N 1N4

and

K. NANDAKUMAR‡

Department of Chemical Engineering, University of Alberta, Edmonton, Alberta, Canada T6G 2G6

Abstract—Multiplicity features of natural convection flow in porous media, generated and sustained by a uniform internal heat source are investigated. The flow, in a two-dimensional enclosure, is described by the Brinkman's extension of the Darcy equation. No-slip boundary conditions are used. The focus is on the role of the Brinkman viscous term in influencing the location of singular points. The behavior of the system is regulated by two control parameters, the Rayleigh number (the dynamic parameter) and the Darcy number. The singular solutions are constructed using algorithms from bifurcation theory. Multiple solutions consisting of symmetric and nonsymmetric solution branches, are revealed as the control parameters change. The range of the Rayleigh number for which a unique solution exists is enlarged when the Darcy number is increased. © 1997 Elsevier Science Ltd.

INTRODUCTION

Over the last three decades, natural convection in fluid-saturated porous media has been studied quite extensively. Numerous authors cite a wide variety of applications involving convective transport in porous media that include utilization of geothermal energy, fiber and granular insulations, design of packed bed reactors and underground disposal of nuclear waste materials. Several others investigate the intricate nature of solution structure from a fundamental point of view in idealized settings.

When a fluid layer is replaced by a fluid-saturated porous layer, the Navier–Stokes equation which is a reliable model for the fluid layer, is replaced by a simpler, but less reliable model for the fluid-saturated porous layer. In fact there are uncertainties about the range of parameters over which a porous media model such as Darcy's equation might remain valid. Even though the model is considerably simpler than the full Navier–Stokes equation, the range of phenomena exhibited by the Darcy model remains rich. Compare for example the richness of the solution structure revealed by Nandakumar and Weinitschke [1] and

Weinitschke *et al.* [2]. Among the earlier works in porous media that have recognized these similarities are those by Lapwood [3], Elder [4], Caltagirone [5] and Kimura *et al.* [6]. Lapwood examined the linear stability of basic conduction state in porous media using Darcy's law which was inspired by the Rayleigh–Benárd problem [7], governed by the Navier–Stokes equations. The ensuing response of the fluid can be quite complicated, particularly when one considers a geometry with a high degree of symmetry. As the degree of forcing (i.e. heating) is increased, the flow structure losses these symmetries spontaneously and the multiplicity of solutions increases.

Since the Darcy model was developed in an empirical manner, questions regarding its universal validity (in the same sense as the validity of the Navier–Stokes equation for fluid layers) has been addressed by numerous authors. Slattery [8] and Whitaker [9] have examined the relationship between the Navier–Stokes equation and the Darcy's law through volume averaging concepts. Beavers and Sparrow [10] have examined the non-Darcy effects, while Beavers and Joseph [11] and Saffman [12] have looked at the boundary conditions for the Darcy model. The phenomenological Darcy equation does not include inertial effects ; nor does it satisfy the no-slip condition at bounding surfaces or porous media. These limitations have been suspected to be the cause of modeling errors under certain circumstances in convective heat trans-

---

† Presently at POSCO Technical Labs, Pohang P.O. Box 36, 1 Koedong-dong, Nam-ku, Pohang-shi, Kyungbuk, Korea, 790-785.
‡ Author to whom correspondence should be addressed.

NOMENCLATURE

a	half-width or half-height of domain [m]		x	direction along the width of domain
A	cross-sectional area [m²]		y	direction along the height of domain.
C_p	specific heat [J (kgK)⁻¹]			
Da	Darcy number (K/a^2)		**Greek symbols**	
D_h	hydraulic diameter [m]		∇	gradient operator
g	acceleration due to gravity [m s⁻²]		∇^2	Laplacian operator
I	identity matrix		α	thermal diffusivity ($k/\rho C_p$) [m² s⁻¹]
k	thermal conductivity [J (msK)⁻¹]		β	coefficient of thermal expansion [K⁻²]
K	permeability [m²]		Ω	vorticity
Nu	Nusselt number (hD_h/k), dimensionless		μ	dynamic viscosity [kg (ms)⁻¹]
O	corrector for Ω, dimensionless		v	kinematic viscosity [m² s⁻¹]
p	pressure [Pa]		Ψ	stream function
P	corrector for Ψ, dimensionless		ρ	density [kg m⁻³]
R	domain of computation		θ	temperature.
r	residual			
Ra	Rayleigh number ($Kg\beta Q_g Aa/K\alpha v$)		**Subscripts, superscripts and other symbols**	
Q_g	heat generation rate per unit volume [W m⁻³]		a	antisymmetric property
			b	bulk quantity
s	arclength parameter		f	fluid property
S	symmetric matrix		s	symmetric property
T	temperature, K or corrector for θ		w	quantity at bounding surfaces of porous media
u	velocity component in x-direction		′	dimensional quantity
v	velocity component in y-direction		*	quantity of null eigenvector
w	weight factor		$\langle\rangle$	averaged quantity.

fer across porous media. To overcome these limitations, the Darcy equation has been extended in an empirical manner by several authors. Amongst others, Forchheimer [13] introduced the inertial term and Brinkman [14] included the viscous force term to the Darcy equation.

Numerous studies [15–18] have focused on the non-Darcy effects using these extended Darcy equations, but they have not examined in detail the multiplicity features of convective flow in porous media. From experimental studies and numerical calculations, it is found that, for the same condition, the patterns of the convective flow in porous. media could vary. That is, multiple solutions through bifurcation are possible. Furthermore, it is likely that the convective flow undergoes complex bifurcation as the buoyancy is increased. The differences in the solutions structure, the location of the singular points (such as limit point, symmetry breaking bifurcation point etc) and the convective flow patterns predicted by various alternate models describing convective flow in porous media could serve as a model discrimination tool, provided a good set of experimental data are available. With this as primary motivation we investigate the detailed solution structure and how it is altered by the inclusion of the Brinkman term.

The present study is concerned with the natural convection flow in porous media within which heat is

uniformly generated. To satisfy the no-slip condition on solid boundaries, the Brinkman's extension of the Darcy equation is employed. The conditions under which the effects of the Brinkman's viscous force term become significant are of primary interest. Construction of multiple steady state solutions are carried out numerically using the algorithms from the recently developed bifurcation theory.

PROBLEM FORMULATION

System description

The system considered in the present study consists of a horizontal, two-dimensional porous medium of width $2a$, height $2a$ and permeability K. The porous medium is saturated with a fluid of density ρ and viscosity μ. There is a uniform internal heat generation per unit volume Q_g and the boundary of the porous medium is maintained at a uniform temperature T'_w. The porous medium is also assumed to be homogenous and isotropic. A sketch of the geometry and coordinate system of the porous medium under study is shown in Fig. 1.

Governing equations

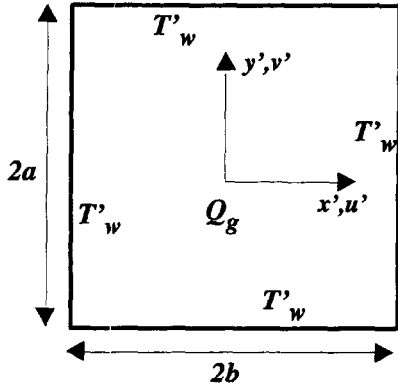The volume-averaged conservation equations of mass, momentum and energy for a two-dimensional flow field are:

Fig. 1. Geometry and coordinate system.

$$\nabla' \cdot \mathbf{v}' = 0 \qquad (1)$$

$$-(\nabla'p' + \rho g) - \frac{\mu}{K}\mathbf{v}' + \mu\nabla'^2\mathbf{v}' = 0 \qquad (2)$$

$$(\mathbf{v}' \cdot \nabla')T' = \alpha\nabla'^2 T' + \frac{Q_g}{(\rho C_p)_f}. \qquad (3)$$

The Boussinesq approximation is invoked to allow for the density variation with temperature in the gravity term of the momentum equation (2) while density in other terms and all other material properties are assumed constant. The reference temperature is T'_w.

$$\rho_f = \rho_w[1 - \beta(T' - T'_w)].$$

Here α is the effective thermal diffusivity, β is the coefficient of thermal expansion and ρ_w is the density at the temperature T'_w. The Brinkman's extension of the Darcy equation, allows for both the no-slip and impermeable boundary conditions to be enforced on the momentum equation (2). For the energy equation (3, no heat transfer resistance between the solid and the fluid phases is assumed. Equations (1)–(3) are to be solved in the two-dimensional region defined by

$$R' := [(x',y')|-a \leqslant x' \leqslant a, \quad -a \leqslant y' \leqslant a].$$

Since the flow is two-dimensional, the stream function, $\Psi(x,y)$ and the vorticity, $\Omega(x,y)$ can be introduced as

$$u' = \frac{\partial\Psi'}{\partial y'}, \quad v' = -\frac{\partial\Psi'}{\partial x'}, \quad \Omega' = \frac{\partial v'}{\partial x'} - \frac{\partial u'}{\partial y'}.$$

Defining the following dimensionless variables,

$$x = x'/a, \quad y = y'/a, \quad u = \frac{u'}{\alpha/a}, \quad v = \frac{v'}{\alpha/a}$$

$$\Psi = \frac{\Psi'}{\alpha}, \quad \Omega = \frac{\Omega'}{\alpha/a^2}, \quad \theta = \frac{(T'_w - T')}{Q_g A/k}.$$

Equations (1)–(3) can be cast in dimensionless, stream function-vorticity form, applicable over the non-dimensional domain, $R := [(x,y)|-1 \leqslant x \leqslant 1, -1 \leqslant y \leqslant 1]$. The final form of the equations are:

$$-Ra\frac{\partial\theta}{\partial x} + \Omega - Da\nabla^2\Omega = 0 \qquad (4)$$

$$\nabla^2\Psi + \Omega = 0 \qquad (5)$$

$$\nabla^2\theta - \frac{\partial\Psi}{\partial y}\frac{\partial\theta}{\partial x} + \frac{\partial\Psi}{\partial x}\frac{\partial\theta}{\partial y} + 1/4 = 0 \qquad (6)$$

where the control parameters appearing in equations (4)–(6) are defined as, $Ra = Ka\beta Q_g Aa/k\alpha\nu$ and $Da = K/a^2$. Once the temperature field is obtained, the average Nusselt number, a useful scalar measure of the system performance, can be obtained from the following overall energy balance

$$Q_g(A\Delta z) = h(\Delta z)8a(T'_b - T'_w)$$

where Δz is the depth perpendicular to the x–y plane and h is the heat transfer coefficient. From the definition of the Nusselt number hD_h/k

$$Nu = \frac{Q_g AD_h}{k8a}\frac{1}{\langle(T'_b - T'_w)\rangle}.$$

The above equation in the dimensionless form becomes

$$Nu = \frac{1}{2}\frac{1}{\langle\theta_b\rangle} \qquad (7)$$

where the bulk mean temperature is

$$\langle\theta_b\rangle = \int_R \theta\,dx\,dy/A.$$

Symmetry and boundary conditions

The governing equations (4)–(6) have the following symmetry features.

$$u(-x,y) = -u(x,y), \quad v(-x,y) = v(x,y)$$

$$\Psi(-x,y) = -\Psi(x,y), \quad \Omega(-x,y) = -\Omega(x,y),$$

$$\theta(-x,y) = \theta(x,y).$$

Therefore, the boundary conditions on the line of symmetry ($x = 0$) are

$$\Psi = 0, \quad \Omega = 0, \quad \frac{\partial\theta}{\partial x} = 0.$$

These can be used for the computation of the symmetric solutions over the half domain $R^+ := [(x,y)|0 \leqslant x \leqslant 1, -1 \leqslant y \leqslant 1]$.

On the solid boundary, the Dirichlet type boundary conditions are used for the temperature and the stream function $\theta = 0$, $\Psi = 0$ while the values of the vorticity are obtained by taking the Taylor series expansion for the stream function [19].

NUMERICAL METHODS

Calculation of regular solutions

The nonlinear boundary value problem defined by equations (4)–(6) can be represented as

$$F(\mathbf{u}, Ra, Da) = 0 \tag{8}$$

where $\mathbf{u} := (\theta(x,y), \Omega(x,y), \Psi(x,y))$. The nonlinear equation (8) can be solved by using the Newton–Raphson method in which the successive correctors,

$$\mathbf{U}_n = (T(x,y), O(x,y), P(x,y))$$

are sought by solving the linear boundary value problem

$$F_\mathbf{u}(\mathbf{U}_n, Ra, Da)\mathbf{U}_n = \mathbf{r}_n \tag{9}$$

Where F_u is the Fréchét derivative. The explicit form of the equations represented by equation (9) and derived from equations (4)–(6) are,

$$-Ra\frac{\partial T}{\partial x} + O - Da\nabla^2 O = r_1 \tag{10}$$

$$\nabla^2 P + O = r_2 \tag{11}$$

$$\nabla^2 T - \frac{\partial\Psi}{\partial x}\frac{\partial T}{\partial y} + \frac{\partial P}{\partial x}\frac{\partial\theta}{\partial y} = r_3 \tag{12}$$

where r_1, r_2, r_3 are the residuals of equations (4)–(6). The solution for the linear boundary value problem equations (10)–(12) can be easily obtained for $Ra = 0$ by using the zero profile as a predictor $\mathbf{u}_0$. Then, the predictor which is needed for the next step $Ra + \Delta Ra$ can be generated by employing the Euler–Newton method

$$\mathbf{u}(Ra + \Delta Ra) = \mathbf{u}(Ra) + \frac{\partial\mathbf{u}}{\partial Ra}\Delta Ra$$

where $\partial\mathbf{u}/\partial Ra$ is obtained from

$$F_\mathbf{u}(\mathbf{u}, Ra, Da)\frac{\partial\mathbf{u}}{\partial Ra} = -\frac{\partial F}{\partial Ra}.$$

When there is a limit point nearby, the regular continuation scheme fails. This can be overcome by parametrizing the problem with the pseudoarclength parameter s, measured along the solution path. Then, the dynamic parameter Ra is treated as an element of the unknown vector $(\theta(s), \Omega(s), \Psi(s), Ra(s))$. Various parametrizing equations have been proposed in the literature. We use the one similar to that proposed by Keller [20]. namely

$$w\int\int [(\theta(s) - \theta(s_0))^2 + (\Omega(s) - \Omega(s_0))^2$$

$$+ (\Psi(s) - \Psi(s_0))^2]\,dx\,dy$$

$$+ (1 - w)(Ra(s) - Ra(s_0))^2 = (s - s_0)^2 \tag{13}$$

where w is a weight factor, used to give equal weight to all of the variables that go to define the arclength.

Calculation of singular points

Two frequently observed singular points in nonlinear phenomena are the limit point (or a turning point) and a symmetry breaking bifurcation point. At a limit point, a solution branch comes from one side and turns back. A simple quadratic limit point can be located by solving the following extended system which was proposed by Moore and Spence [21] and Spence and Werner [22]

$$F(\mathbf{u}, Ra, Da) = 0, \quad F_\mathbf{u}(\mathbf{u}, Ra, Da)\mathbf{v} = 0, \quad l(\mathbf{v}) = 1 \tag{14}$$

where $\mathbf{v} = (\theta^*, \Omega^*, \Psi^*)$ is the right null vector and the constraint $l(\mathbf{v}) = 1$ forces the right null vector to be non-trivial. The extended system is not singular and can be solved by using the Newton–Raphson method. Solving the extended system of equations (14) means that the nonlinear equations (4)–(6) must be solved simultaneously with, $F_\mathbf{u}(\mathbf{u}, Ra, Da)\mathbf{v} = 0$ and $l(\mathbf{v}) = 1$ for the unknowns $(\theta, \Omega, \Psi, \theta^*, \Omega^*, \Psi^*, Ra)$. The extended system, equation (14) is solved over the half domain R^+ for limit points that lie on the symmetric solution branches and over the full domain R for limit points on the asymmetric solution branches.

Symmetry breaking bifurcation may be described as the bifurcation in which the solutions on one of the two intersecting branches are symmetric while the solutions on the other branch are asymmetric. The symmetry S is defined by

$$\mathbf{S} \neq \mathbf{I}, \quad \mathbf{S} = \mathbf{I}^2, \quad F(\mathbf{Su}, Ra, Da) = \mathbf{S}F(\mathbf{u}, Ra, Da).$$

Werner and Spence [23] showed that the pitchfork type symmetry breaking bifurcation point can be located by solving the same extended system equations (14) with the restriction $\mathbf{u} \in \mathbf{X}_s$, $\mathbf{v} \in \mathbf{X}_a$ where $\mathbf{X}_s$ and $\mathbf{X}_a$ represent the symmetric subspace, $[\mathbf{u}|\mathbf{Su} = \mathbf{u}]$ and antisymmetric subspace, $[\mathbf{u}|\mathbf{Su} = -\mathbf{u}]$, respectively.

Discretization

The partial differential equations, equations (10)–(12) were discretized using finite difference approximations in the half domain R^+ for symmetric solutions and the full domain R for the asymmetric solutions, respectively. The central difference scheme was used over a uniform grid where the grid points were numbered as $[(x_i, y_j)|i = 0, \ldots, N+1, \ j = 0, \ldots, M+1]$. For symmetric solutions, the discretized five-point formulae used in the interior of the grid were also used on the boundary $[(0, y_j)|j = 0, \ldots, M+1]$. This introduces an extra set of points outside the domain of interest which is eliminated by imposing the following symmetry conditions

$$T_{-1,j} = T_{1,j}, \quad O_{-1,j} = -O_{1,j}, \quad P_{-1,j} = -P_{1,j}.$$

The system of the finite difference equations yields a sparse matrix in which most of the elements are zero. To solve the sparse matrix at every Newton–Raphson step efficiently, the sparse matrix solver, SPARSPAK [24] was used.

RESULTS AND DISCUSSION

The physical mechanism and the nonlinearities that are responsible for the complex multiple solutions structure in any problem of natural convection are reasonably well understood. It is the embellishments caused by specific features (in the present case the effect of nonzero Darcy number, Da or the effects of the Brinkman term) that interests us. The domain of interest is a closed system into which there is no net flow. The two competing forces are the viscous and buoyancy forces. When the dynamic parameter, Ra is small enough that the viscous force dominates, there is a unique and stable solution. However, as Ra is increased, the strength of buoyancy is increased and it destabilizes the flow field. In this way, additional solutions bifurcate from the unique solution at certain critical values of Ra. The spatial symmetries that are broken within the constraint of two-dimensionality are also tracked.

Recognizing that several different solutions can coexist at a certain Ra, a uniform grid which is fine enough to resolve all the details of different solution structures is used. For this, grid sensitivity tests were carried out at selected parameters and the results are shown in Table 1. Assuming the approximation

Table 1. Grid sensitivity tests: (a) Richardson extrapolation of Nusselt number for $Da = 0.0$, $Ra = 3000$; (b) grid sensitivity test at regular points for $Da = 0$, $Ra = 5000$. AS1* was computed on (40×40) and (60×60); (c) variation of singular points with grid refinement for $Da = 0$, $Ra = 5000$

(a)

Grid	Spacing	Nusselt number
5×10	0.10	12.2873
10×20	0.05	12.3074
15×30	0.03333	12.4027
20×40	0.025	12.4374
25×50	0.02	12.4537
30×60	0.01667	12.4627
extrapolated	0.0	12.4716

(b)

	Nusselt number Grid	
Branch	(20×40)	(30×60)
PM1	15.2354	15.2860
IS1 high	14.6704	14.7446
IS1 low	12.2466	14.2809
AS1*	14.1360	14.1945

(c)

	Ra Grid	
Singular point	(20×40)	(30×60)
L1	2856.03	2569.77
SB1	4165.57	4237.56
L2	4166.41	4238.12
L3	4507.78	4436.06

$u \approx u(h) + ch^2$, where u is the exact solution and c is a constant independent of the grid spacing h, the Richardson extrapolation scheme is used to obtain the solution at $h = 0$. Table 1(a) shows that the computed Nusselt numbers for $h = 0.025 \sim 0.01667$ have less than 1% deviation from the Nusselt number obtained from the extrapolation. In Tables 1(b) and (c), comparisons of Nusselt numbers on various solution branches and singular points for the two different grid spacing $h = 0.025$ and 0.01667 are shown. As the grid is refined from $h = 0.025$ to 0.01667, Nusselt numbers on the various solution branches at $Ra = 5000$ differ by less than 1%. The location of the singular points, Ra change by less than 2%. These tests provide a measure of the accuracy of our numerical results. It is important to note that the overall solution structure in terms of the number of singular points and the interconnections of solution branches remained unchanged. Therefore, to keep the computational costs modest, all of the computations for this parametric study were made using a grid spacing of $h = 0.025$, which is equivalent to the grids of (20×40) and (40×40) for the symmetric and the asymmetric solutions, respectively.

Solution structure for $Da = 0$

The Darcy model can be viewed as a special case of the more general Brinkman's model. When $Da \rightarrow 0$, the Brinkman viscous force term in equation (4) vanishes and equation (4) is reduced to the Darcy equation. Note that the order of the equation decreases in the limit of $Da \rightarrow 0$, thus making it impossible to satisfy the no-slip condition. Although this limiting case has been investigated in detail by Weinitshke *et al.* [2], the solution branches were reconstructed to verify the code and the results are summarized here so that they can be compared with the results for $Da \neq 0$.

Figure 2 shows the solution structure which consists of various solution branches for $Da = 0$ and up to $Ra = 10,000$. Expanded scales, used in Fig 2(b,c), reveal the detailed structure. The dotted lines are nonsymmetric solutions and they occur in pairs, with one being the mirror image of the other. Since Nu is an averaged quantity both parts of an asymmetric branch have the same value and, hence, they appear as a single curve in these bifurcation diagrams. A unique solution on the primary branch, PM1 was easily obtained for $Ra = 0$ and then the entire branch of PM1 was generated using the arclength continuation scheme over the half domain R^+. The first asymmetric solution branch, AS1, which bifurcates at the two symmetry breaking bifurcation points, SB1 and SB2, was found by introducing asymmetric perturbation to the Euler–Newton method over the full domain R. The isolated symmetric solution branches, IS1 and IS2, and the asymmetric solution branches, AS2 and AS3 were generated in the same way. The singular points, namely the limit points and symmetry breaking points, were located by solving the extended sys-
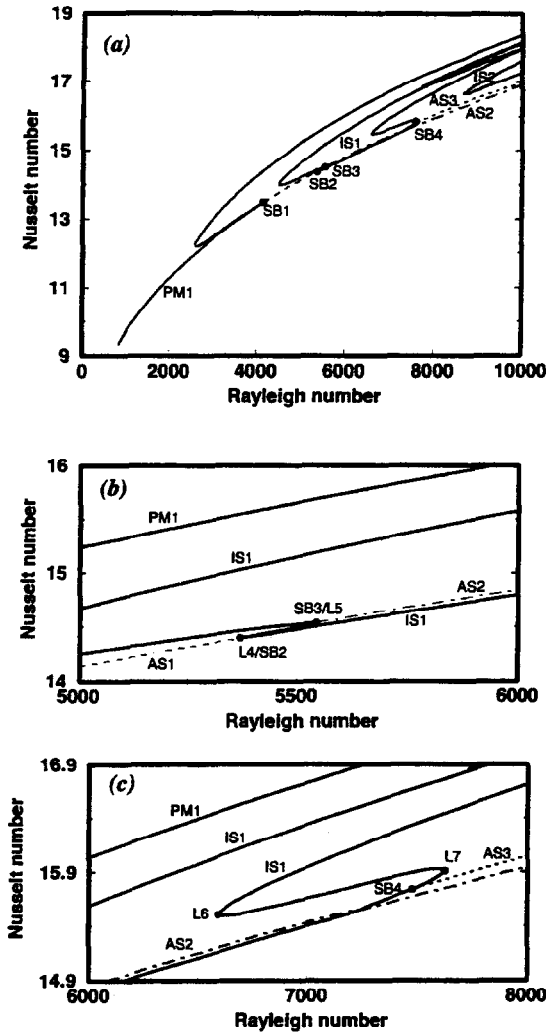
Table 2. Singular points for $Da = 0.0$

Singular point	Branch	Rayleigh number
L1	PM1	2586.03
SB1	PM1 and AS1	4165.57
L2	PM1	4166.41
L3	IS1	4507.78
L4	IS1	5369.95
SB2	IS1 and AS1	5370.53
SB3	IS1 and AS2	5542.19
L5	IS1	5542.38
L6	IS1	6594.96
SB4	IS1 and AS3	7468.92
L7	IS1	7622.09
L8	IS1	7728.29
L9	IS2	8651.91
L10	IS1	9917.02

Fig. 2. Bifurcation diagram with Nusselt number as the state variable and Rayleigh number as the parameter for a fixed Darcy number of $Da = 0$ is seen in (a). Additional details of the bifurcation diagram are revealed by zooming in over $Ra \in [5000, 6000]$ in (b) and over $Ra \in [6000, 8000]$ in (c). PM1 refers to the primary solution branch, ISn refers to symmetric solution branches, ASn refers to asymmetric branches, Ln refers to limit points and SBn refers to symmetry breaking bifurcation points.

tem equation (14) and the Ra values of the singular points are listed in Table 2. It is seen that all the symmetry breaking bifurcations happen near the limit points. This phenomenon was also reported for Lapwood convection [25] and the Morton problem [1]. However, the limit points and the symmetry breaking bifurcation points do not coincide since the symmetry breaking bifurcation occurs as a pitchfork.

The stability test for each solution branch was also carried out. If any eigenvalue of the matrix from the Fréchét derivative at a certain Ra has a positive real part, the solution at the Ra is considered unstable. In this study, the simple power iteration method combined with the scheme which maps all the eigenvalues with negative real parts onto the unit circle was used

to monitor the stability numerically. The lower part and the upper part of PM1 are stable, but the middle part of PM1, the solution path between L1 and L2, is not stable. The stable lower and the upper parts of PM1 are analogous to those observed by Buretta and Berman [26] in their experiment. They reported an apparent discontinuity in the heat transfer curve for various permeable beds. They correctly postulated that the discontinuous jump in the heat transfer rate is a bifurcation phenomenon and multiple solutions must exist. This is the only known experimental observation of bifurcation phenomena in porous media. The observations were on macroscopic quantity like the Nusselt number and not on the flow patterns or velocity fields. In the present study, multiple solutions start to appear beyond $Ra = 2586.03$ (L1 in Table 2). Our interest is to examine how this structure unfolds for nonzero Da. Note that the upper branch is only conditionally stable. It is unstable to non-symmetric perturbations.

Solution structure for $Da = 10^{-4}$

The Brinkman viscous force term in equation (4) now plays a role in determining the solution structure, permitting the no-slip conditions to be satisfied. Note that non-zero values of Da do not influence the symmetries in the system. The solution structure for $Da = 10^{-4}$ is shown in Fig. 3. The overall solution structure in Fig. 3 looks similar to that in Fig. 2 in terms of the number of solution branches and their interconnection. The precise location of the singular points Ra are given in Table 3. It is seen that the singular points in Table 3 move to higher values of Ra compared with those in Table 2.

A new branching behavior is locally observed in Fig. 3. The limit points which correspond to L7 and L9 in Fig. 2 disappear in Fig. 3 through a transcritical bifurcation. With the extended system formulations of equation (14) such structural changes in the connectivity of the branches could be easily tracked by simply continuing the solution of equation (14) in a
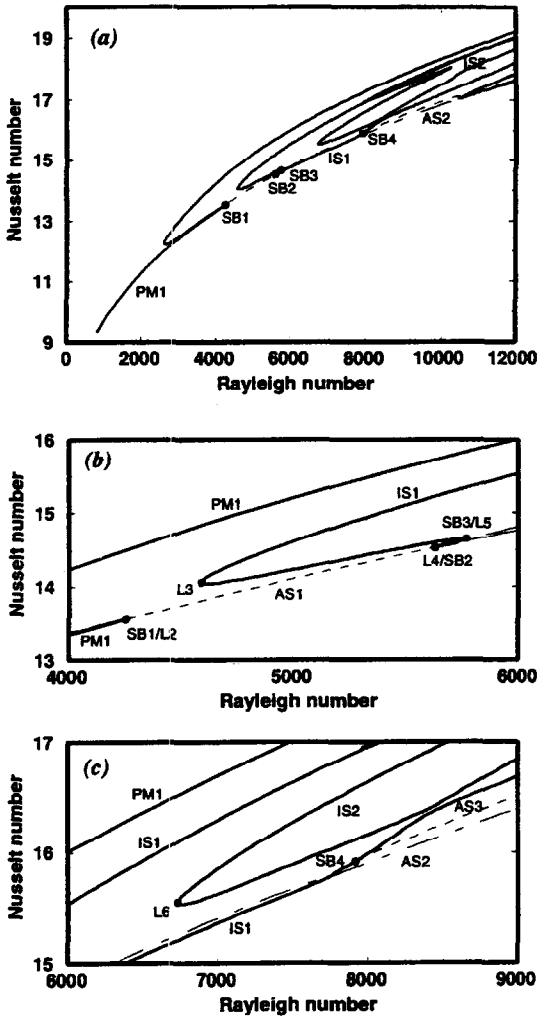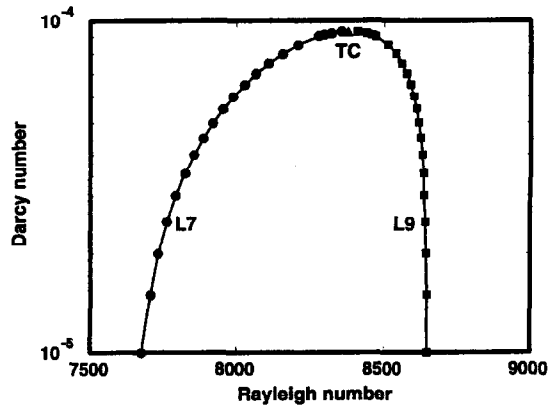
Fig. 4. Limit points L7 and L9 coalesce at a transcritical bifurcation point TC.

closer and then disappear between $Da = 0.93 \times 10^{-4}$ and $Da = 0.94 \times 10^{-4}$ at the transcritical point labeled TC in Fig. 4. There are other extended system formulations that allow the precise computation of the point TC in the two parameter problem (Ra, D) and implementing such schemes would be useful if we are interested in tracking how the point TC changes with changes in a third parameter. For our purpose Fig. 4 provides sufficient details on the structural changes. Figure 5 shows the bifurcation diagrams just before $(Da = 0.93 \times 10^{-4})$ and after $(Da = 0.94 \times 10^{-4})$ the transcritical bifurcation. Note that the limit points, L7 and L9 are very close in Fig. 5(a). The unstable branches IS1m and IS2u in Fig. 5(a) merge into the unstable branch IS2 in Fig. 5(b) through the transcritical bifurcation. In the same way, the stable branches IS1d and IS2d in Fig 5(a) merge into the stable branch IS1 in Fig. 5(b). Changing Da can be

Fig. 3. (a) Bifurcation diagram for a Darcy number of $Da = 10^{-4}$. Additional details of the bifurcation diagram are revealed by zooming in over $Ra \in [4000, 6000]$ in (b) and over $Ra \in [6000, 9000]$ in (c). Labels are as in Fig. 2.

second parameter such as Da. Figure 4 shows the unfolding of the limit points, L7 and L9 with the change of Da. As Da is increased, L7 and L9 come

Table 3. Singular points for $Da = 10^{-4}$

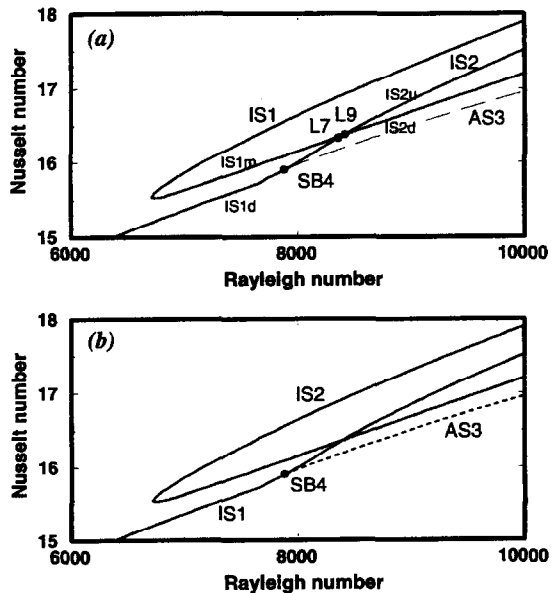| Singular point	Branch	Rayleigh number
L1	PM1	2612.72
SB1	PM1 and AS1	4256.61
L2	PM1	4257.53
L3	IS1	4587.74
L4	IS1	5627.30
SB2	IS1 and AS1	5628.14
SB3	IS1 and AS2	5765.65
L5	IS1	5765.99
L6	IS2	6726.30
SB4	IS1 and AS3	7917.26
L7	IS2	7960.55
L8	IS2	10264.36
L9	IS3	10458.79

Fig. 5. Unfolding of the bifurcation diagram around a transcritical (TC) point. (a) just before TC at a Darcy number of $Da = 0.93 \times 10^{-4}$ and (b) just after TC at a Darcy number of $Da = 0.94 \times 10^{-4}$.

considered as a perturbation which does not affect the symmetry feature of the given system. Therefore, the symmetry breaking bifurcation point SB4 remains robust even if L7 which locates nearby SB4 disappears after the transcritical bifurcation.

Solution structure for Da $= 10^{-3}$

The solution structure for $Da = 10^{-3}$ is shown in Fig. 6(a) for $Ra \in [0, 15000]$ and expanded versions of the state diagram are shown in Fig 6(b,c) to reveal the details of the interconnection. The precise Ra values of the singular points are given in Table 4. As Da is increased from 10^{-4} to 10^{-3}, a pitchfork bifurcation occurs between isolated symmetric solution branches IS1 and IS2. The middle part of IS1 which connects the upper and the lower part of IS1 in Fig. 3 breaks up and then IS1 and IS2 exchange branches. As a result, the upper part of IS1 in Fig. 3 appears as IS2 in Fig. 6. In Fig. 7, the bifurcation diagrams just before $(Da = 0.7 \times 10^{-3})$ and after $(Da = 0.8 \times 10^{-3})$
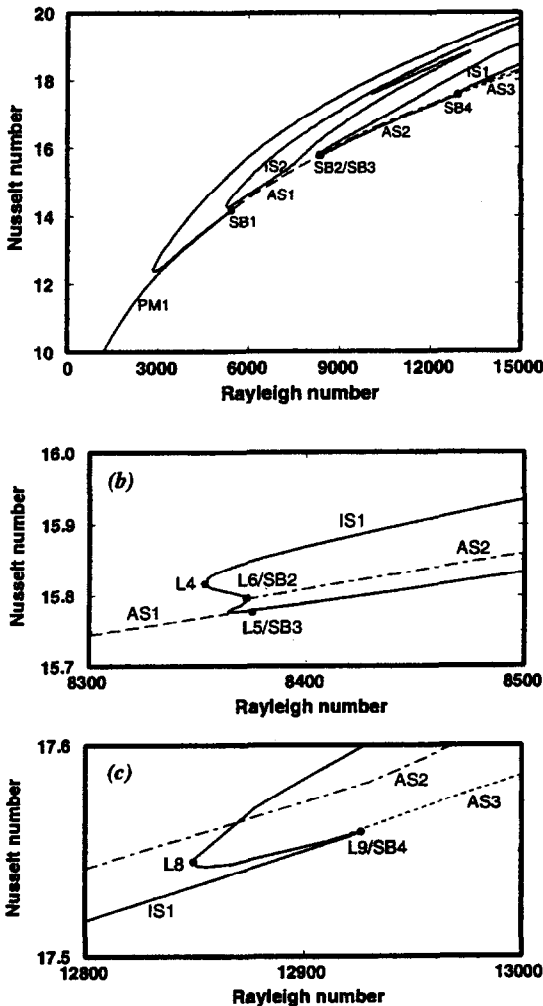

Fig. 6. (a) Bifurcation diagram for a Darcy number of $Da = 10^{-3}$. Additional details of the bifurcation diagram are revealed by zooming in over $Ra \in [8300, 8500]$ in (b) and over $Ra \in [12,800, 13,000]$ in (c). Labels are as in Fig. 2.

the pitchfork bifurcation are shown. IS1 and IS2 approach each other as Da is increased in Fig. 7(a). At certain value of Da, IS1 and IS2 connect with each other. Eventually, IS1l and IS2u in Fig. 7(a) merge into IS2 in Fig. 7(b) while IS1r and IS2d in Fig. 7(a) merge into IS1 in Fig. 7(b).

Each of the different solution branches in the bifurcation diagram corresponds to different flow patterns. Across any singular point, there is a qualitative change in the flow pattern. In Fig. 6, a total of five different solutions are found at $Ra = 7000$. Three symmetric solutions are on PM1 and IS2 and two asymmetric solutions are on AS1. Since the asymmetric solutions occur in pairs in which one is the mirror image of the other, AS1 in Fig. 6 represents two different asymmetric solutions. The contours of the streamlines and isotherms for the five different solutions are shown in Fig. 8. It is seen that the upper part of PM1 and the upper part of IS2 have four-vortex flow patterns while the lower part of IS2 and AS1 have two-vortex flow patterns.

Below Ra value of the first limit point L1, there is only one solution branch which gives a unique solution. The variation of L1 with Da was traced and the result is shown in Fig. 9. Upon increasing Da, L1 moves to higher values of Ra. The feature of multiple solutions appear at higher values of Ra as Da is increased. Therefore, it is conjectured that the Brinkman viscous force term acts as an additional damping mechanism which retards bifurcations to multiple solutions.

Finally, the effects of Da on heat transfer rates are shown in Fig. 10. The curves in Fig. 10(a,b) represent the lower part of PM1 and the upper part of PM1, respectively. As can be seen in Fig. 10, the Nusselt number decreases as Da is increased for a given value of Ra and the deviation is larger at a higher Ra.

CONCLUSIONS

A numerical study of natural convection in square, two-dimensional porous media with a uniform volumetric heating has been presented. The Brinkman's extension of the Darcy equation and a single energy equation are employed to describe the system. The multiplicity feature of the problem has been resolved using algorithms from bifurcation theory. Complete solution branches are tracked using the arclength continuation scheme combined with the Newton–Raphson method. Limit points and symmetry breaking bifurcation points are also calculated solving the extended system. From qualitative changes of solution structures and unfoldings of singular points with variation of Da, the non-Darcy characteristics of the given problem have been investigated. A transcritical bifurcation is found at Da between 0.93×10^{-4} and 0.94×10^{-4}. A pitchfork bifurcation is found on isolated symmetric solution branches at Da between 0.7×10^{-3} and 0.8×10^{-3}. The bifurcation which leads to multiple solution from a unique solution occurs at
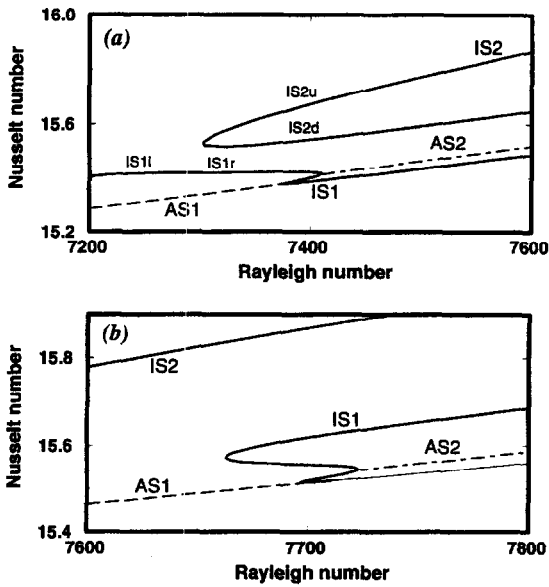
Fig. 7. Unfolding of the bifurcation diagram around a pitch-fork (PF) bifurcation point. (a) just before PF at a Darcy number of $Da = 0.7 \times 10^{-3}$ and (b) just after PF at a Darcy number of $Da = 0.8 \times 10^{-3}$.
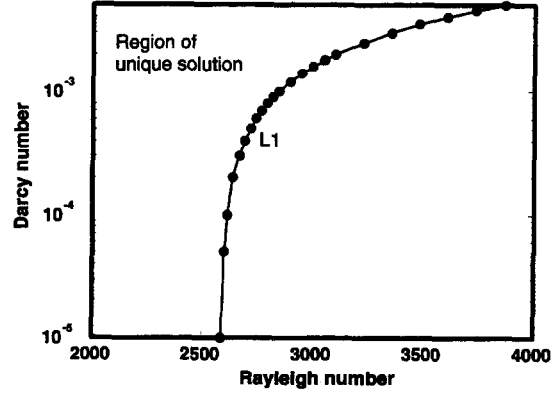

Fig. 9. Variation in the limit point L1 with Darcy number which demarcates the uniqueness region.
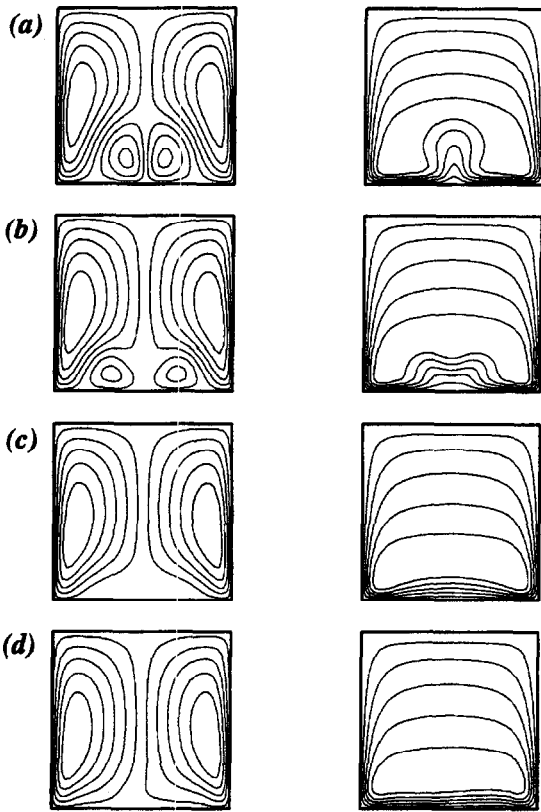

Fig. 8. Five different solutions exist at $Ra = 7000$ and $Da = 10^{-3}$. Contours of streamlines (left) and isotherms (right) are shown for each solution. (a) Four-vortex pattern on PM; (b) four-vortex pattern on the upper part of IS2, (c) two-vortex pattern on the lower part of IS2, and (d) asymmetric two-vortex pattern on AS1.
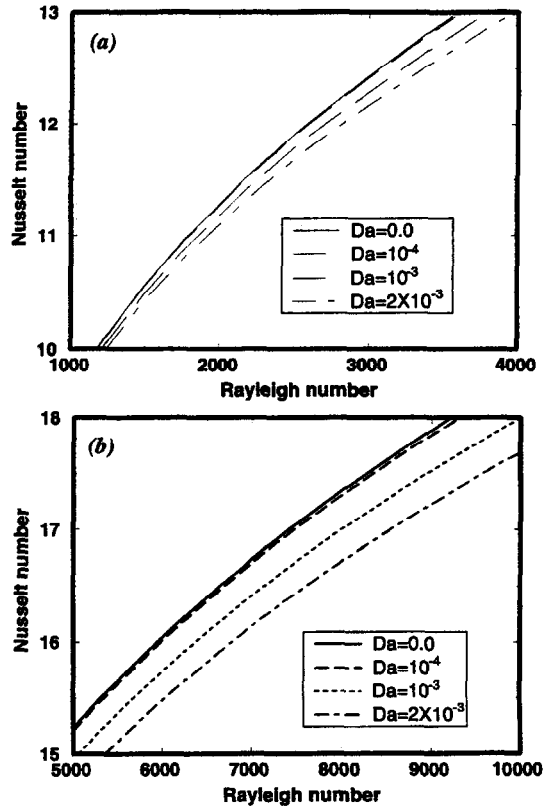

Fig. 10. Nusselt number vs Rayleigh number for various Da. (a) On the lower part of PM1; and (b) on the upper part of PM1.

Table 4. Singular points for $Da = 10^{-3}$

Singular point	Branch	Rayleigh number
L1	PM1	2845.13
SB1	PM1 and AS1	5418.32
L2	IS2	5242.63
L3	PM1	5420.68
L4	IS1	8352.88
L5	IS1	8363.71
SB2	IS1 and AS2	8372.66
L6	IS1	8372.72
SB3	IS1 and AS1	8375.11
L7	IS2	10058.51
L8	IS1	12848.94
SB4	IS1 and AS3	12913.91
L9	IS1	12926.34
L10	IS2	13342.03

higher values of Ra as Da is increased. Heat transfer rates decrease as Da is increased.

REFERENCES

1. Nandakumar, K. and Weinitschke, H. J., A bifurcation study of mixed-convection heat transfer in horizontal ducts. *Journal of Fluid Mechanics*, 1991, **231**, 157.
2. Weinitschke, H. J., Nandakumar, K. and Ravi Sankar, S., A bifurcation study of convective heat transfer in porous media. *Physics of Fluids A*, 1990, **2**, 912.
3. Lapwood, E. R., Convection of a fluid in a porous medium. *Proceedings of the Cambridge Philosophical Society*, 1948, **44**, 508.
4. Elder, J. W., Steady free convection in a porous medium heated from below. *Journal of Fluid Mechanics*, 1967, **27**, 29.
5. Caltagirone, J. P., Thermoconvective instabilities in a horizontal porous layer. *Journal of Fluid Mechanics*, 1975, **72**, 169.
6. Kimura, S., Schubert, G. and Straus, J. M., Route to chaos in porous-medium thermal convection. *Journal of Fluid Mechanics*, 1986, **166**, 305.
7. Benárd, H., Les tourbillons cellulaires dans une nappe liquide transportant de la chaleur par convection en régime permanant. *Annales de Chimie et de Physique*, 1901, 7 (Ser. 23), 62.
8. Slattery, J. C., Single-phase flow through porous media. *AIChE Journal*, 1969, **15**, 866.
9. Whitaker, S., The equations of motion in porous media. *Chemical Engineering Science*, 1967, **21**, 291.
10. Beavers, G. S. and Sparrow, E. M., Non-Darcy flow through fibrous porous media. *Transactions of the ASME Journal of Applied Mechanics*, 1969, **36**, 711.
11. Beavers, G. S. and Joseph, D. D., Boundary conditions at a naturally permeable wall. *Journal of Fluid Mechanics*, 1967, **30**, 197.
12. Saffman, P. G., On the boundary conditions at the surface of a porous medium. *Studies in Applied Mathematics*, 1971, **50**, 93.
13. Forchheimer, P. H., *Zeitschrift ver Deutscher Ingineur*, 1901, **45**, 1782.
14. Brinkman, H. C., A calculation of the viscous force extended by a flowing fluid on a dense swarm of particles. *Applied Scientific Research*, 1947, **A1**, 27.
15. Chan, B. K. C., Ivey, C. M. and Barry, J. M., Natural convection in enclosed porous media with rectangular boundaries. *Transactions of the ASME Journal of Heat Transfer*, 1970, **92**, 21.
16. Vafai, K. and Tien, C. L., Boundary and inertia effects on flow and heat transfer in porous media. *International Journal of Heat and Mass Transfer*, 1981, **24**, 195.
17. Tong, T. W. and Subramanian, E., A boundary-layer analysis for natural convection in vertical porous enclosures—use of the Brinkman-extended Darcy model. *International Journal of Heat and Mass Transfer*, 1985, **28**, 563.
18. Gill, U. S. and Minkowycz, W. J., Boundary and inertia effects on conjugate mixed convection heat transfer from a vertical plate fin in a high-porosity porous medium. *International Journal of Heat and Mass Transfer*, 1988, **31**, 419.
19. Roache, P. J., *Computational Fluid Dynamics*. Hermosa, 1972.
20. Keller, H. B., *Applications of Bifurcation theory*, ed. P. H. Rabinowitz. Academic, New York, 1977.
21. Moore, G. and Spence, A., The calculation of turning points of non-linear equations. *SIAM Journal of Numerical Analysis*, 1980, **17**, 567.
22. Spence, A. and Werner, B., Non-simple turning points and cusps. *IMA Journal of Numerical Analysis*, 1982, **2**, 413.
23. Werner, B. and Spence, A., The computation of symmetry breaking bifurcation points. *SIAM Journal of Numerical Analysis*, 1984, **21**, 388.
24. Chu, E., George, A., Liu, J. and Ng, E., Department of Computer Science, University of Waterloo, SPARSPAK Research Report no. CS-84-36, 1984.
25. Riley, D. S. and Winters, K. H., Modal exchange mechanisms in Lapwood convection. *Journal of Fluid Mechanics*, 1989, **204**, 325.
26. Buretta, R. J. and Berman, A. S., Convection heat transfer in a liquid saturated porous layer. *Transactions of the ASME Journal of Applied Mechanics*, 1976, **43**, 249.